INTERNATIONAL JOURNAL FOR NUMERICAL METHODS IN FLUIDS
Int. J. Numer. Meth. Fluids 2006; **50**:147–164
Published online 15 September 2005 in Wiley InterScience (www.interscience.wiley.com). DOI: 10.1002/fld.1048

On accurate boundary conditions for a shape sensitivity equation method

R. Duvigneau[1,*,†] and D. Pelletier[2,‡]

[1]*Laboratoire de Mecanique des Fluides CNRS UMR 6598, Ecole Centrale de Nantes, Nantes, France*
[2]*Département de Génie Mécanique, Ecole Polytechnique de Montréal, P.O. Box 6079, Station Centre-Ville Montréal, Québec, Canada H3C 3A7*

SUMMARY

This paper studies the application of the continuous sensitivity equation method (CSEM) for the Navier–Stokes equations in the particular case of shape parameters. Boundary conditions for shape parameters involve flow derivatives at the boundary. Thus, accurate flow gradients are critical to the success of the CSEM. A new approach is presented to extract accurate flow derivatives at the boundary. High order Taylor series expansions are used on layered patches in conjunction with a constrained least-squares procedure to evaluate accurate first and second derivatives of the flow variables at the boundary, required for Dirichlet and Neumann sensitivity boundary conditions. The flow and sensitivity fields are solved using an adaptive finite-element method. The proposed methodology is first verified on a problem with a closed form solution obtained by the Method of Manufactured Solutions. The ability of the proposed method to provide accurate sensitivity fields for realistic problems is then demonstrated. The flow and sensitivity fields for a NACA 0012 airfoil are used for fast evaluation of the nearby flow over an airfoil of different thickness (NACA 0015). Copyright © 2005 John Wiley & Sons, Ltd.

KEY WORDS: continuous sensitivity equation method; shape sensitivity; boundary derivatives reconstruction; adaptive FEM; Navier–Stokes

1. INTRODUCTION

Sensitivity analysis is used for a wide range of engineering problems. Contrary to adjoint approaches [1–3], which only exist within the context of an optimization problem, sensitivities exist on their own. While they find uses in design optimization [4], they can be used for non-optimization purposes, such as characterization of complex flows, uncertainty analysis [5], fast evaluation of nearby flows, etc. Sensitivity information can be obtained in two ways. In the *approximate-then-differentiate* approach (often called discrete sensitivity equation method), the discrete form of the flow equations are differentiated and the total derivative of the flow

*Correspondence to: R. Duvigneau, Laboratoire de Mecanique des Fluides CNRS UMR 6598, Ecole Centrale de Nantes, Nantes, France.
†E-mail: Regis.Duvigneau@ec-nantes.fr
‡E-mail: Dominique.Pelletier@polymtl.ca

Received 30 November 2004
Revised 16 June 2005
Accepted 21 June 2005

discretization with respect to the design parameters is calculated. In the *differentiate-then-approximate* approach (known as the continuous sensitivity equation method (CSEM)), partial differential equations for the flow sensitivities are obtained by implicit differentiation of the equations governing the flow. They are then approximated numerically.

The CSEM is preferred for the present study, because it offers several advantages over the discrete sensitivity approach. In particular, since differentiation occurs before any discretization, the delicate computation of mesh sensitivities and all of the overhead associated with them is avoided. Although automatic differentiation can be used to generate the necessary terms in formulating the CSE, the CSEM requires less memory and is computationally less expensive than automatic differentiation, as shown by Borggaard and Verma [6]. Moreover, the CSEM is a natural approach when using adaptive methods: since the topology of the mesh changes with adaptation, mesh derivatives do not exist, making the discrete sensitivity method ill-suited. Another advantage is that there is no requirement to use the same algorithm to approximate the CSE and the original PDE model. Thus, special algorithms can be constructed to take advantage of the linear structure of the CSE.

However, the main difficulty with the CSEM arises when one deals with shape parameters. In this particular case, flow gradients are required as source terms in the CSE and as coefficients in the boundary conditions for the CSE. Flow gradients in the interior of the computational domain can be computed relatively easily and accurately by a local projection technique [7] (which is already used for error estimation). However, on general unstructured meshes, the accuracy of reconstructed derivatives degrades significantly near the boundary [8]. This induces errors in the boundary conditions that result in poor solutions for the sensitivity fields (the numerical solution often appears shifted from the exact solution by some fixed amount that varies from one problem to the next).

The current study presents a new approach to extract accurate boundary conditions of the CSE for shape parameters. It uses high order Taylor series expansions in conjunction with a constrained least-squares procedure. The proposed approach is first verified on a boundary layer flow problem with a closed form solution obtained by the method of manufactured solutions (MMS) [8, 9]. The MMS provides a rigorous framework to precisely quantify the numerical errors. Flows around airfoils are then considered to illustrate the ability of the proposed method to deal with realistic problems. The CSEM is used for fast evaluation of nearby flows via linear Taylor series in parameter space. The flow and sensitivity fields computed around a NACA 0012 airfoil are used to evaluate the flow around a NACA 0015 airfoil, by considering the airfoil thickness as a shape parameter. The extrapolated flow obtained is compared to the true flow computed around a NACA 0015 airfoil.

2. FLOW EQUATIONS

The flows of interest are described by the laminar steady Navier–Stokes equations. The mass, momentum and energy conservation laws are written as

$$\rho \mathbf{u} \cdot \nabla \mathbf{u} = -\nabla p + \nabla \cdot \{\mu(\nabla \mathbf{u} + (\nabla \mathbf{u})^{\mathrm{T}})\} - \rho \mathbf{g} \beta (T - T_0) + \mathbf{f} \tag{1}$$

$$\nabla \cdot \mathbf{u} = 0 \tag{2}$$

$$\rho c_p \mathbf{u} \cdot \nabla T = \nabla \cdot (\kappa \nabla T) + q \tag{3}$$

using the Boussinesq approximation, where ρ is the density, μ the viscosity, $\mathbf{u}$ the velocity, p the pressure, T the temperature, $\mathbf{g}$ the gravity, β the bulk expansion coefficient, c_p the specific heat, T_0 a reference temperature and κ the conductivity. Finally, $\mathbf{f}$ and q are volumetric forces and heat source, respectively.

Dirichlet and Neumann boundary conditions are imposed on boundaries Γ_{D} and Γ_{N}, respectively,

$$T = \bar{T} \quad (\Gamma_{\mathrm{D}}^{\mathrm{T}}) \tag{4}$$

$$\kappa \nabla T \cdot \hat{\mathbf{n}} = \bar{q} \quad (\Gamma_{\mathrm{N}}^{\mathrm{T}}) \tag{5}$$

$$\mathbf{u} = \bar{\mathbf{u}} \quad (\Gamma_{\mathrm{D}}^{u}) \tag{6}$$

$$[-p\mathbf{I} + \mu(\nabla \mathbf{u} + (\nabla \mathbf{u})^{\mathrm{T}})] \cdot \hat{\mathbf{n}} = \bar{\mathbf{t}} \quad (\Gamma_{\mathrm{N}}^{u}) \tag{7}$$

where $\hat{\mathbf{n}}$ is an outward unit vector normal to the boundary and $\mathbf{I}$ the second-order identity tensor.

3. CONTINUOUS SENSITIVITY EQUATIONS

The continuous sensitivity equations (CSE) are derived formally by implicit differentiation of the flow equations (1)–(3) with respect to an arbitrary parameter a. Thus, we treat the variable $\mathbf{u}$ as a function of both space and parameter a. This dependence is denoted $\mathbf{u} = \mathbf{u}(\mathbf{x}; a)$. The flow sensitivities are defined as the following partial derivatives:

$$\mathbf{s}_{\mathbf{u}} = \frac{\partial \mathbf{u}}{\partial a}, \quad s_p = \frac{\partial p}{\partial a}, \quad s_T = \frac{\partial T}{\partial a} \tag{8}$$

Then, with no particular assumption on the nature of the parameter a, the CSEs governing the sensitivity fields are written as

$$\begin{aligned} \rho' \mathbf{u} \cdot \nabla \mathbf{u} + \rho(\mathbf{s}_{\mathbf{u}} \cdot \nabla \mathbf{u} + \mathbf{u} \cdot \nabla \mathbf{s}_{\mathbf{u}}) = & -\nabla s_p + \nabla \cdot \{\mu'(\nabla \mathbf{u} + (\nabla \mathbf{u})^{\mathrm{T}})\} \\ & + \nabla \cdot \{\mu(\nabla \mathbf{s}_{\mathbf{u}} + (\nabla \mathbf{s}_{\mathbf{u}})^{\mathrm{T}})\} \\ & - \rho' \mathbf{g} \beta (T - T_0) - \rho \mathbf{g}_a \beta (T - T_0) \\ & - \rho \mathbf{g} \beta' (T - T_0) - \rho \mathbf{g} \beta (s_T - (T_0)_a) \\ & + \mathbf{f}_a \end{aligned} \tag{9}$$

$$\nabla \cdot \mathbf{s}_{\mathbf{u}} = 0 \tag{10}$$

$$(\rho' c_p + \rho c_p') \mathbf{u} \cdot \nabla T + \rho c_p (\mathbf{s}_{\mathbf{u}} \cdot \nabla T + \mathbf{u} \cdot \nabla s_T) = \nabla \cdot (\kappa \nabla s_T + \kappa' \nabla T) + q_a \tag{11}$$

$\mathbf{g}_a$, $(T_0)_a$, $\mathbf{f}_a$ and q_a are the partial derivatives of $\mathbf{g}$, T_0, $\mathbf{f}$ and q in Equations (1) and (3). The total derivatives of the fluid properties with respect to the parameter a are denoted using a ($'$).

For instance

$$\mu' = \frac{\mathrm{D}\mu}{\mathrm{D}a} = \frac{\partial \mu}{\partial a} + \frac{\partial \mu}{\partial \mathbf{u}} \cdot \mathbf{s_u} + \frac{\partial \mu}{\partial T} s_T \tag{12}$$

To complete the description of the problem, the boundary conditions (5)–(6) are differentiated in the same manner. However, if a is a shape parameter, the position of the boundary is parameter dependent. Then, the differentiation must account for the fact that both the boundary location and the value of the boundary condition depend on a. Therefore, the boundary conditions for the CSE are

$$s_T = \bar{T}' - \nabla T \cdot \frac{\partial \mathbf{x}}{\partial a} \quad (\Gamma_{\mathrm{D}}^{\mathrm{T}}) \tag{13}$$

$$(\kappa' \nabla T + \kappa \nabla s_T) \cdot \hat{\mathbf{n}} = \bar{q}' - \left\{ \nabla(\kappa \nabla T) \cdot \frac{\partial \mathbf{x}}{\partial a} \right\} \cdot \hat{\mathbf{n}} - \kappa(\nabla T) \cdot \frac{\partial \hat{\mathbf{n}}}{\partial a}, \quad (\Gamma_{\mathrm{N}}^{\mathrm{T}}) \tag{14}$$

$$\mathbf{s_u} = \bar{\mathbf{u}}' - \nabla \mathbf{u} \cdot \frac{\partial \mathbf{x}}{\partial a} \quad (\Gamma_{\mathrm{D}}^{u}) \tag{15}$$

$$\begin{aligned} &[-s_p \mathbf{I} + \mu(\nabla \mathbf{s_u} + (\nabla \mathbf{s_u})^{\mathrm{T}})] \cdot \hat{\mathbf{n}} + [\mu'(\nabla \mathbf{u} + (\nabla \mathbf{u})^{\mathrm{T}})] \cdot \hat{\mathbf{n}} \\ &\quad = \bar{\mathbf{t}}' - \left\{ \nabla[-p\mathbf{I} + \mu(\nabla \mathbf{u} + (\nabla \mathbf{u})^{\mathrm{T}})] \cdot \frac{\partial \mathbf{x}}{\partial a} \right\} \cdot \hat{\mathbf{n}} \\ &\qquad -[-p\mathbf{I} + \mu(\nabla \mathbf{u} + (\nabla \mathbf{u})^{\mathrm{T}})] \cdot \frac{\partial \hat{\mathbf{n}}}{\partial a} \quad (\Gamma_{\mathrm{N}}^{u}) \end{aligned} \tag{16}$$

As can be seen, when shape parameters are considered, the first derivatives of the flow variables at the boundary are needed to evaluate sensitivity Dirichlet boundary conditions and second derivatives are required for sensitivity Neumann boundary conditions. This introduces significant numerical challenges and difficulties when solving the CSE. Since approximate boundary conditions are constructed from the finite-element solution for the flow field, inaccuracies in the boundary conditions will result in poor solutions for the sensitivity fields.

4. NUMERICAL FRAMEWORK

4.1. Solver

The flow equations as well as CSE are solved using an adaptive finite-element method [10, 11]. One notices that the cost of implementing the CSE resolution is modest, since the CSE share the same structure and boundary condition type as the original flow problem. We discuss the salient features here for completeness and to set up the approximation of the above-described CSE. The weak form of the continuity, momentum and energy equations are formed, and

a discretization based on the 7-noded Crouzeix–Raviart element pair leads to a system of nonlinear algebraic equations which are then solved using Newton's method.

The accuracy of finite-element approximation is directly related to the element mesh size used. An adaptive remeshing procedure is employed to improve this approximation by refining the mesh in regions of rapid variations of the flow variables. The regions targeted for refinement are identified by using an error estimator based on local projections of discontinuous quantities onto a local continuous polynomial basis [7, 12]. For example, since the Crouzeix–Raviart element pair uses quadratic basis functions for velocity and temperature, the quantities τ and $\kappa\nabla T$ are both discontinuous and piecewise linear for this approximation. By projecting these derivatives onto a continuous quadratic polynomial basis, we can define an error estimate by measuring the difference between the reconstructed and finite-element derivatives.

Once error estimates are obtained for all dependent variables, an optimal mesh is designed using the asymptotic convergence rate of the finite-element method. An optimal mesh is generated which redistributes the mesh sizes so that each element bears the same contribution to the total error (i.e. equidistribution of the error norm). This is performed in an iterative fashion, beginning with a coarse mesh and producing progressively finer meshes, by reducing the error by a constant factor from one mesh to the next. Details of this adaptive remeshing procedure may be found in the literature [13].

4.2. Boundary conditions for CSE

As explained above, flow boundary derivatives are required by the CSE boundary conditions for shape parameters. The local projection of flow derivatives, used for errors estimation [7, 12], may be employed to provide the boundary derivatives. However, this approach yields poor results since projected derivatives usually exhibit low accuracy at the boundary, as shown in the previous work of Turgeon *et al.* [4, 8]. To improve the evaluation of the flow derivatives at the boundary, we propose to use high order Taylor series expansions around each boundary vertex. The method to extract flow derivatives using a least-squares method was demonstrated by Fortin *et al.* [14]. We innovate by enforcing constraints on the least-squares method to ensure that the Taylor series are consistent with the boundary conditions.

For the sake of simplicity, the proposed method is presented for a generic flow variable ϕ. The truncated Taylor series expansion of order k for the flow variable ϕ around a boundary node $P(x_p, y_p)$ reads

$$\begin{aligned}\phi(x,y) = \phi(x_p,y_p) + (x-x_p)\phi_x + (y-y_p)\phi_y \\ + \tfrac{1}{2}(x-x_p)^2\phi_{xx} + (x-x_p)(y-y_p)\phi_{xy} + \tfrac{1}{2}(y-y_p)^2\phi_{yy} + \cdots\end{aligned} \tag{17}$$

in which ϕ and its derivatives are the unknowns. Their values are determined by matching, in a least-squares sense, the value of the Taylor series to that of the flow variable at a set of points $N(x_n, y_n)$ within a patch $\mathscr{P}$ surrounding the node P. This corresponds to solving the following overdetermined rectangular system of equations:

$$\phi_N = \mathbf{B}^{\mathrm{T}}\mathbf{y}_\phi \quad \forall N \in \mathscr{P} \tag{18}$$

where

$$\phi_N = \phi(x_n, y_n) \tag{19}$$

$$\mathbf{B}^{\mathrm{T}} = \{1 \;\; x_n - x_p \;\; y_n - y_p \;\; \tfrac{1}{2}(x_n - x_p)^2 \;\; (x_n - x_p)(y_n - y_p) \;\; \tfrac{1}{2}(y_n - y_p)^2 \ldots\} \tag{20}$$

$$\mathbf{y}_\phi^{\mathrm{T}} = \{\phi \;\; \phi_x \;\; \phi_y \;\; \phi_{xx} \;\; \phi_{xy} \;\; \phi_{yy} \ldots\}_P \tag{21}$$

To determine $\mathbf{y}_\phi$, a discrete least-squares problem is solved by minimizing the square of the distance between the Taylor series and the value of the variable at the N mesh nodes in the patch $\mathscr{P}$. That is we minimize the quadratic form $\mathscr{J}(\mathbf{y}_\phi)$

$$\mathrm{Min}\, \mathscr{J}(\mathbf{y}_\phi) = \frac{1}{2} \sum_{N \in \mathscr{P}} (\mathbf{B}^{\mathrm{T}} \mathbf{y}_\phi - \phi_N)^2 \tag{22}$$

The boundary condition for ϕ at node P is either a Dirichlet condition $\phi = \overline{\phi_P}$ or a Neumann condition $\nabla\phi \cdot \hat{n} = \overline{q_P}_\phi$. However, there is no guarantee that the Taylor series (17) evaluated at the boundary node P will match the boundary condition. Further accuracy improvements are achieved if the least-squares solution $\mathbf{y}_\phi$ is constrained to match the value of the boundary condition at node P. The boundary condition is then considered as a constraint for the least-squares problem. One may propose to constrain the least-squares solution to match the value of the boundary condition at all boundary nodes of the patch. However, this will result in a too large a number of constraints for the degree of the Taylor series.

In the case of a Dirichlet boundary condition $\phi = \overline{\phi_P}$, we now minimize $\mathscr{J}(\mathbf{y}_\phi)$ subject to $\mathbf{y}_\phi(1) = \overline{\phi_P}$. The constraint is enforced by introducing a Lagrange multiplier l_ϕ so that the resulting least-squares problem reads

$$\mathrm{Min}\, \mathscr{J}_D(\mathbf{y}_\phi) = \frac{1}{2} \sum_{N \in \mathscr{P}} (\mathbf{B}^{\mathrm{T}} \mathbf{y}_\phi - \phi_N)^2 + l_\phi(\mathbf{D}_\phi^{\mathrm{T}} \mathbf{y}_\phi - \overline{\phi_P}) \tag{23}$$

where $\mathbf{D}_\phi^{\mathrm{T}} = \{1 \; 0 \; 0 \; \ldots \; 0\}$. By setting the gradients of (23) to zero, we obtain the following linear system for $\mathbf{y}_\phi$:

$$\begin{bmatrix} \sum_{N \in \mathscr{P}} \mathbf{B}\mathbf{B}^{\mathrm{T}} & \mathbf{D}_\phi \\ \mathbf{D}_\phi^{\mathrm{T}} & 0 \end{bmatrix} \begin{Bmatrix} \mathbf{y}_\phi \\ l_\phi \end{Bmatrix} = \begin{Bmatrix} \sum_{N \in \mathscr{P}} \mathbf{B}\phi_N \\ \overline{\phi_P} \end{Bmatrix} \tag{24}$$

whose solution is obtained by LU factorization. In the case of a Neumann boundary condition $\nabla\phi \cdot \hat{n} = \overline{q_P}_\phi$, we thus minimize the quadratic form $\mathscr{J}(\mathbf{y}_\phi)$ subject to $\mathbf{y}_\phi(2)\hat{n}_x + \mathbf{y}_\phi(3)\hat{n}_y = \overline{q_P}_\phi$

$$\mathrm{Min}\, \mathscr{J}_N(\mathbf{y}_\phi) = \frac{1}{2} \sum_{N \in \mathscr{P}} (\mathbf{B}^{\mathrm{T}} \mathbf{y}_\phi - \phi_N)^2 + l_\phi(\mathbf{N}_\phi^{\mathrm{T}} \mathbf{y}_\phi - \overline{q_P}_\phi) \tag{25}$$

with $\mathbf{N}_\phi^{\mathrm{T}} = \{0, \hat{n}_x\hat{n}_y, 0, \ldots, 0\}$. The extremum corresponds to the solution of the following linear system:

$$\begin{bmatrix} \sum_{N \in \mathscr{P}} \mathbf{B}\mathbf{B}^{\mathrm{T}} & \mathbf{N}_\phi \\ \mathbf{N}_\phi^{\mathrm{T}} & 0 \end{bmatrix} \begin{Bmatrix} \mathbf{y}_\phi \\ l_\phi \end{Bmatrix} = \begin{Bmatrix} \sum_{N \in \mathscr{P}} \mathbf{B}\phi_N \\ \overline{q_P}_\phi \end{Bmatrix} \tag{26}$$

First-order boundary derivatives $\mathbf{y}_\phi(2)=\phi_x$ and $\mathbf{y}_\phi(3)=\phi_y$, and second-order boundary derivatives $\mathbf{y}_\phi(4)=\phi_{xx}$, $\mathbf{y}_\phi(5)=\phi_{xy}$ and $\mathbf{y}_\phi(6)=\phi_{yy}$ are then used to evaluate boundary conditions for the CSE. To make the methodology more concrete, we consider in turn the four cases corresponding to the four boundary conditions for the Navier–Stokes equations provided by Equations (13)–(16) in Appendix A.

5. VERIFICATION FOR A BOUNDARY LAYER FLOW

5.1. Problem description

We study the accuracy of the proposed scheme using the MMS [8, 9] for a simple boundary layer flow. The MMS is a rigorous and general procedure to verify the numerical accuracy of a given code. It consists in imposing a closed form solution to a given problem, by modifying the equations that are solved. Since the solution is known analytically, the numerical accuracy can be evaluated by performing a systematic grid refinement study. We use a manufactured solution [15] that behaves like a two-dimensional mixed convection boundary layer along a heated flat plate. This closed form solution provides a rigorous framework to assess the following points:

- The convergence of the flow and its sensitivities to the exact solution with mesh adaptation.
- The loss of accuracy arising from the approximate flow gradients used in the boundary conditions along parameter dependent boundaries.
- The accuracy improvements due to the constrained Taylor least-squares reconstruction of boundary derivatives.
- The effects of the Taylor series order and of the extent of the patch on the global accuracy.

The following expressions are a manufactured solution mimicking mixed convection along a flat plate:

$$U=U_0(1-\mathrm{e}^{-\varepsilon}),\quad V=\frac{U_0}{2\delta\sqrt{x}}(1-(1+\varepsilon)\mathrm{e}^{-\varepsilon}),\quad p=x^2-0.01,\quad T=\Delta T\mathrm{e}^{-\gamma}+T_0 \tag{27}$$

with

$$\varepsilon=(y-y_0)\sqrt{\frac{U_0\rho}{\mu x}},\quad \delta=\sqrt{\frac{U_0\rho}{\mu}},\quad \gamma=\left(\frac{\mu c_p}{\lambda}\right)^n(y-y_0)\sqrt{\frac{\rho U_0}{\mu x}} \tag{28}$$

These expressions are substituted in the flow equations to determine the required source terms to ensure heat and momentum balance. The above solution is then differentiated with respect to y_0 the vertical position of the plate, yielding an exact solution to the sensitivity equations for a shape parameter. The source term for the CSE is the derivative of the flow source term.

For numerical purposes, we choose the following data:

$$U_0=1, \quad \mu=0.01, \quad \Delta T=1, \quad n=\tfrac{1}{3}, \quad y_0=0, \quad T_0=0, \quad \rho=1, \quad c_p=1\lambda=\tfrac{1}{70}, \quad \beta=0.5 \tag{29}$$

The computational domain is the rectangle $[0.1, 1.] \times [0., 1.]$. In our tests, we use Dirichlet boundary conditions on all boundaries for the flow and sensitivity equations. The only exception is at the inlet between $y=0.75$ and 1.0, where the condition $\overline{t_x} = -p + 2\mu(\partial u/\partial x) = 0$ is imposed for the horizontal velocity, and on the plate where the heat flux $q=\kappa(\partial T/\partial y)=\bar{q}$ is prescribed. Thus, two Neumann boundary conditions, one on velocity and one on temperature, are imposed. The Neumann boundary condition for temperature at the wall significantly increases the difficulty of recovering derivatives, because high velocity and temperature gradients are observed at this location.

5.2. *Results*

First, results from previous work, using the local projection method to evaluate boundary derivatives, are presented to underline the poor accuracy of the resulting boundary conditions and the need for improvement [8]. Figure 1 presents the error trajectories and efficiency indices (ratio of global error estimate to the true global error) for the velocity and temperature sensitivities. Notice that the error estimates do not converge to the true errors, yielding poor efficiency indices. This behaviour is due to the presence of numerical errors in the boundary conditions for the CSE, which shifts the solution. This effect cannot be detected by the error estimator. One concludes that error estimates for the CSE in previous work were suboptimal in the case of shape parameters.

To study the influence of the extent of the patch in the present approach, we introduce the concept of an l-layer patch. A 1-layer patch includes all elements that are connected to a given node P, a 2-layer patch includes elements which are connected to elements of the 1-layer patch of node P, etc ... Figure 2 provides two examples of 2-layer patches, one for a vertex node and another for a mid-side node.

Figures 3(a)–6(b) show the error trajectories and efficiency indices for the velocity and temperature sensitivities obtained with the proposed approach, increasing the order of the Taylor series and the size of the patches. As can be seen, poor results are obtained using 4th-order (degree 3) Taylor series expansions. In fact, efficiency indices are worse than those obtained using the local projection method. Improvements are detected with Taylor series of order 5 (degree 6), although asymptotic exactness is not achieved. Better behaviour is obtained with Taylor series of order 6 and 7 (degree 5 and 6): asymptotic exactness of the estimator can be clearly seen. This is confirmed by the curves of the efficiency indices which asymptote to one. These results can be explained by considering the order of accuracy of the boundary condition: when a Neumann boundary condition for the CSE is imposed, the second derivatives of the flow variables are included in the boundary condition. Thus, if 4th-order Taylor series expansions are used for the flow, the boundary condition is only 2nd-order accurate. Then, the accuracy of the boundary condition is lower than that of the finite-element method used (3rd-order), which explains the poor results obtained in this case.

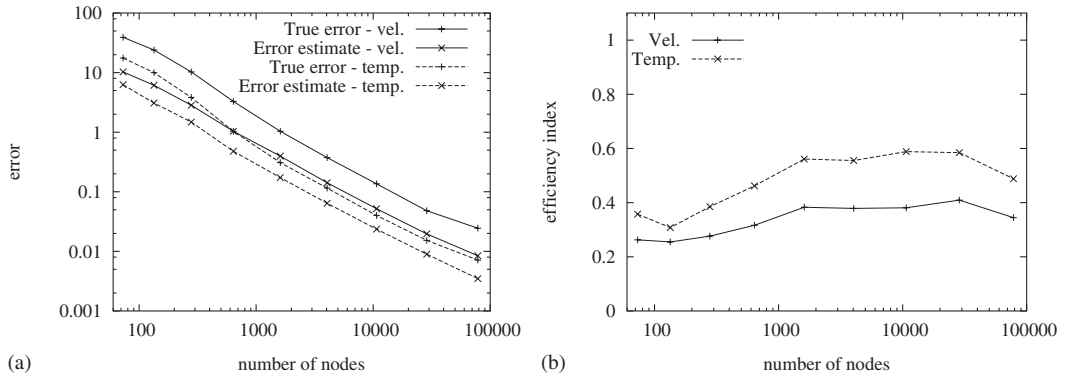

Figure 1. Grid convergence results using the local projection method: (a) error trajectories; and (b) efficiency indices.

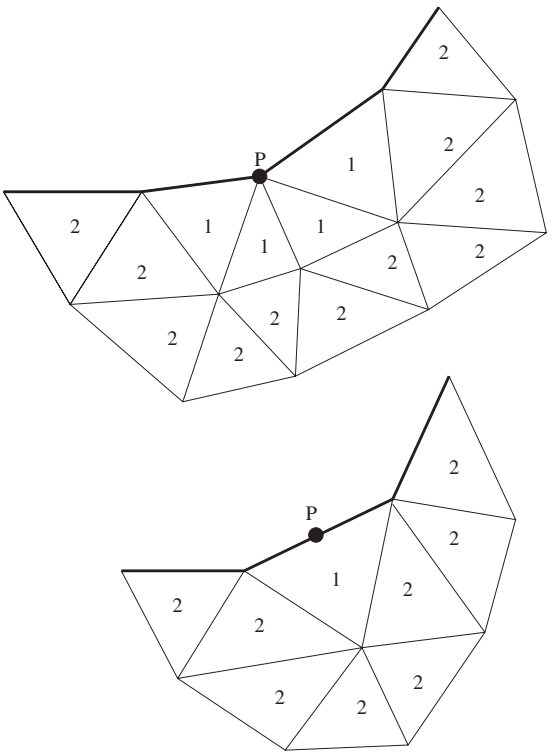

Figure 2. Typical 2-layer patches around node *P*.

On the other hand, when Taylor series expansions of order higher than 5 are used for the flow, the accuracy of the boundary condition is higher than that of the finite-element method, yielding asymptotic exactness of the solution and the error estimator.

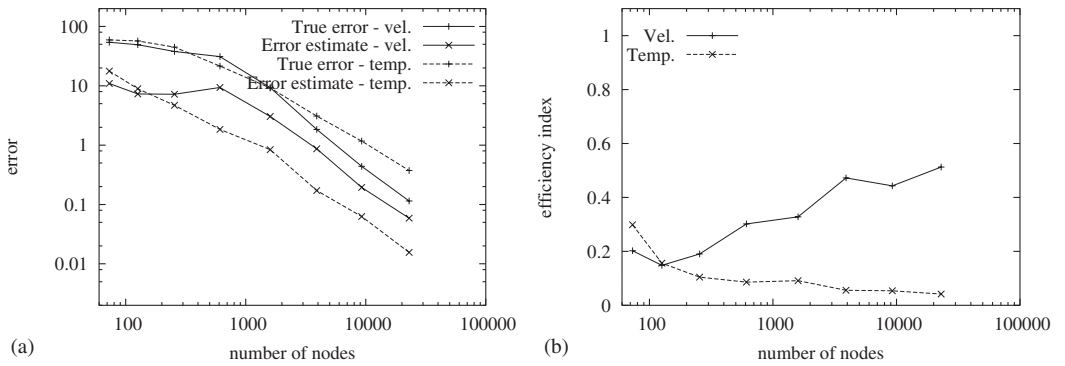

Figure 3. Grid convergence results using 4th-order Taylor series expansions on 5-layer patches: (a) errors; and (b) efficiency indices.

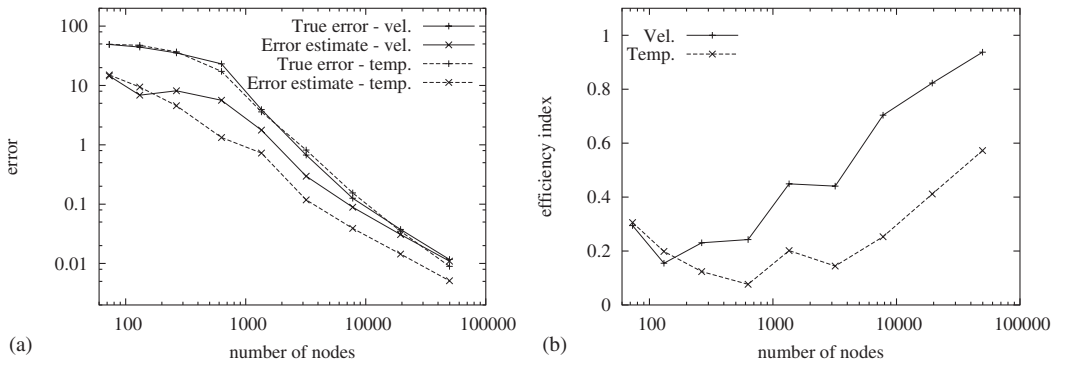

Figure 4. Grid convergence results using 5th-order Taylor series expansions on 6-layer patches: (a) errors; and (b) efficiency indices.

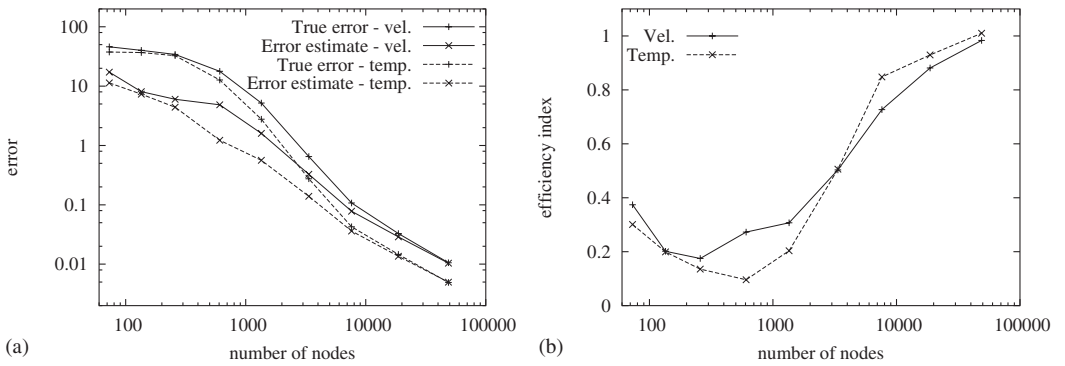

Figure 5. Grid convergence results using 6th-order Taylor series expansions on 7-layer patches: (a) errors; and (b) efficiency indices.

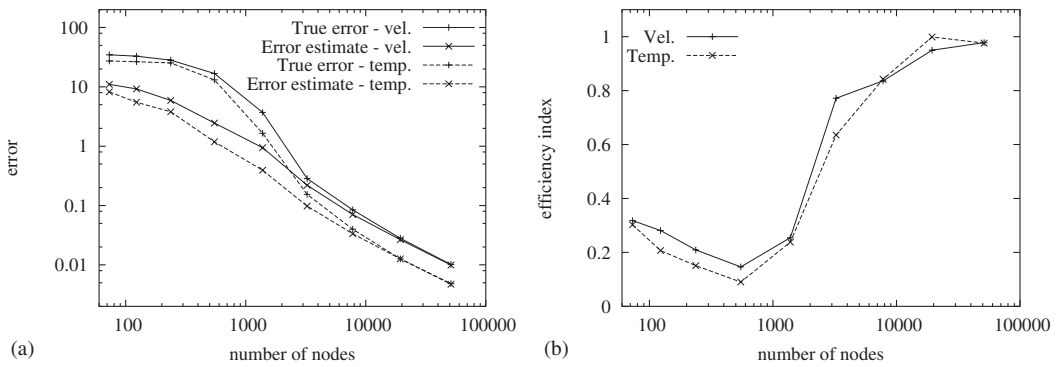

Figure 6. Grid convergence results using 7th-order Taylor series expansions on 8-layer patches: (a) errors; and (b) efficiency indices.

6. APPLICATION TO EVALUATION OF NEARBY AIRFOIL FLOWS

6.1. Problem description

Now, we apply the proposed method to realistic airfoil problems at low Reynolds numbers. We use sensitivity information to estimate nearby solutions for airfoils of different thickness. The flow around a NACA 0012 airfoil at a Reynolds number $Re = 2000$ and an incidence angle of $\alpha = 5^\circ$ is used as a baseline flow and geometry. Dirichlet boundary conditions are imposed at the inflow and on the airfoil surface (no-slip boundary condition), and zero Neumann boundary conditions are prescribed as far field conditions.

The points on a NACA 0012 airfoil verify the following equation:

$$y_t = \pm 5t(0.2969\sqrt{x} - 0.1260x - 0.3537x^2 + 0.2843x^3 - 0.1015x^4) \quad x \in [0,1] \tag{30}$$

with $t = 0.12$ the thickness. In this section, t is treated as a shape parameter. The solutions at nearby values of the parameter t are obtained by evaluating linear Taylor series extrapolations in t-space, using the flow and sensitivity data from the baseline condition. The following expressions are used to predict the flow around the airfoil with a modified thickness:

$$\begin{aligned} u_{\text{NACA 00XX}} &\approx u_{\text{NACA 0012}} + \left(\frac{\partial u}{\partial t}\right) \times \Delta t \\ v_{\text{NACA 00XX}} &\approx v_{\text{NACA 0012}} + \left(\frac{\partial v}{\partial t}\right) \times \Delta t \\ p_{\text{NACA 00XX}} &\approx p_{\text{NACA 0012}} + \left(\frac{\partial v}{\partial t}\right) \times \Delta t \end{aligned} \tag{31}$$

Hence, fast estimates of the flow around the airfoil with a modified thickness can be obtained. To illustrate the capability of the proposed method to evaluate accurate sensitivity fields, the flow around a NACA 0015 airfoil is predicted using the flow and sensitivity data obtained from the baseline NACA 0012 airfoil. The extrapolated flow is then compared to the true flow around a NACA 0015 airfoil obtained from a new separate adaptive computation.

6.2. Results

Calculations are performed using 4th- to 7th-order Taylor series expansions and 4- to 8-layer patches to evaluate boundary derivatives. The contours of S_u obtained using these different parameters are plotted in Figure 7. As can be seen, the choice of order of Taylor series and extent of the patch appear to have little influence on the contours of S_u. Fourth-order Taylor series expansions provide satisfactory results in this case, since only Dirichlet boundary conditions are imposed on the parameter dependent boundary. Eight grid adaptation cycles are performed, the last mesh containing roughly 40 000 nodes. All flow and sensitivity variables contribute to the error estimation and mesh adaptation processes. From here on we only present results obtained with 7th-order Taylor series expansions and 8-layer patches.

Figure 8 shows the baseline pressure coefficient along the surface of the NACA 0012 airfoil, its extrapolation to that of a NACA 0015 airfoil and the pressure coefficient from a flow analysis of a NACA 0015 airfoil. As can be seen, the agreement is very good. The pressure coefficient on the pressure side of the airfoil is predicted very accurately. For the suction side, trends are well predicted. However, for the suction peak, there is a slight discrepancy between the Taylor series and the reanalysis. This indicates that the pressure coefficient dependency in terms of t is more linear on the pressure side than on the suction side of the airfoil.

Figure 9 shows comparisons for the pressure fields, for the NACA 0012 baseline, its Taylor series extrapolation to a NACA 0015 and from reanalysis for a NACA 0015 airfoil. Although large flow modifications appear during the shape changes, a very satisfactory agreement is obtained between the extrapolated pressure field and the pressure field obtained from a new computation.

The velocity field is characterized by a large recirculation zone near the trailing edge of the airfoil. The size and shape of the recirculation are influenced by the thickness of the airfoil. Therefore, these characteristics are demanding criteria to assess the capability of the

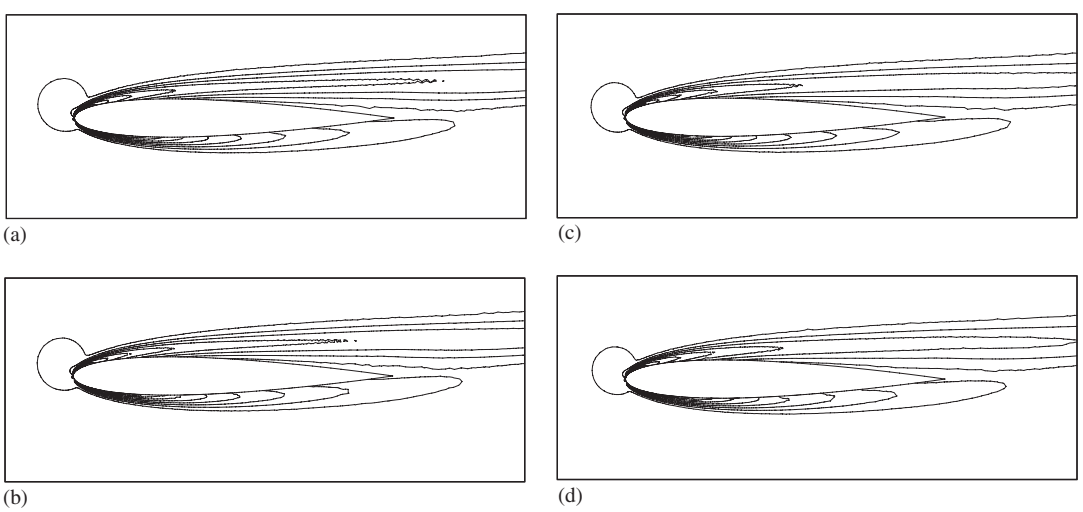

Figure 7. Effects of Taylor series order on S_u: (a) 4th-order on 4-layer patches; (b) 5th-order on 6-layer patches; (c) 6th-order on 7-layer patches; and (d) 7th-order on 8-layer patches.

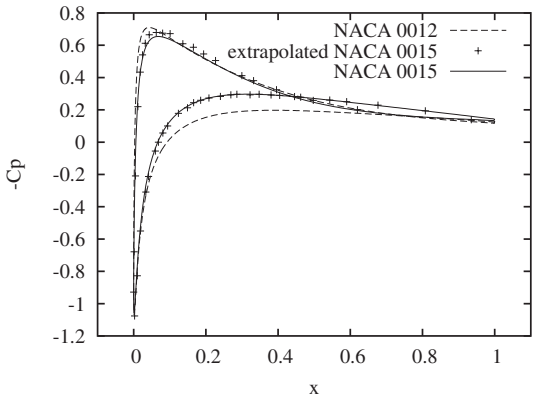

Figure 8. Comparison of the pressure coefficient.

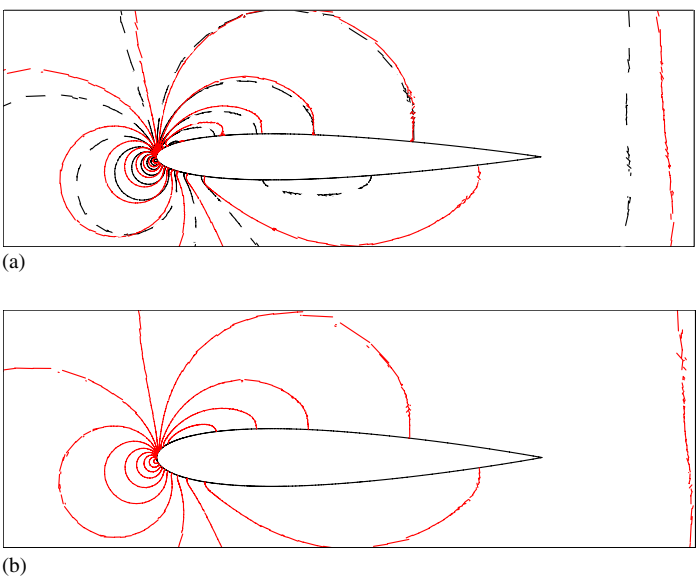

Figure 9. Comparison of pressure contours: (a) NACA 0012 (dashed) and extrapolated NACA 0015 (solid); and (b) NACA 0015.

proposed approach to predict nearby solutions. Figure 10 shows the streamlines for the different computations. For the baseline NACA 0012 airfoil (Figure 10(a)), a large recirculation zone is observed on the suction side close to the trailing edge. A second smaller recirculation is also present just downstream of the trailing edge. The Taylor series estimate for a NACA 0015 airfoil predicts the size increase for the two recirculation bubbles (Figure 10(b)). The upper bubble is shifted upwards as the lower bubble increases in length. Results from a flow reanalysis around a NACA 0015 airfoil is shown in Figure 10(c). As can be seen from

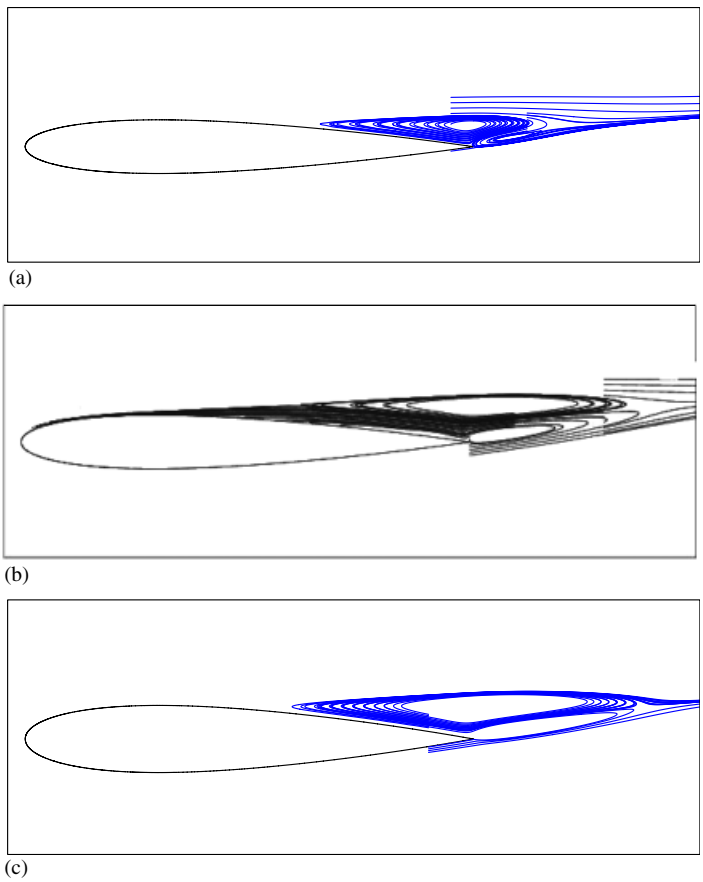

Figure 10. Comparison of streamlines in the recirculation zone: (a) NACA 0012; (b) extrapolated NACA 0015; and (c) NACA 0015.

Figures 10(b) and (c), the characteristics of the recirculation zones are well predicted by the Taylor series extrapolation. Particularly, the changes of the length and shape of the recirculation zone are accurately predicted by the sensitivities.

7. CONCLUSION

A CSEM has been developed for shape parameters. We introduced a Taylor series l-patch constrained least-squares procedure to evaluate the boundary flow gradients which appear in the CSE boundary conditions. Flow and sensitivity fields were solved using an adaptive finite-element method.

Adaptive grid refinement studies were performed using the MMS. For a simple boundary layer flow, the proposed Taylor series l-patch approach provides accurate boundary conditions for CSE. More specifically, it is sufficiently accurate to ensure asymptotic exactness of the error estimator with adaptive mesh refinement.

The proposed approach was then applied to fast evaluation of nearby flow solutions around NACA airfoils of varying thickness. Satisfactory results were obtained when the thickness is considered as a shape parameter. The ability of the proposed method to predict the modifications of the pressure field or the wake characteristics due to thickness changes was demonstrated.

According to this study, the asymptotic exactness of the sensitivity fields and the error estimator for shape parameters can be obtained, if the accuracy of the boundary conditions for CSE is higher than that of the numerical methods used in the solver.

APPENDIX A

A.1. Dirichlet condition for the temperature

When the variable ϕ considered is the temperature and a Dirichlet boundary condition $T = \overline{T_P}$ is imposed at node P, the constrained least-squares problem (24) obviously yields

$$\begin{bmatrix} \sum_{N\in\mathscr{P}} \mathbf{B}\mathbf{B}^{\mathrm{T}} & \mathbf{D}_T \\ \mathbf{D}_T^{\mathrm{T}} & 0 \end{bmatrix} \begin{Bmatrix} \mathbf{y}_T \\ l_T \end{Bmatrix} = \begin{Bmatrix} \sum_{N\in\mathscr{P}} \mathbf{B} T_N \\ \overline{T_P} \end{Bmatrix} \tag{A1}$$

with

$$\mathbf{y}_T^{\mathrm{T}} = \{T \;\; T_x \;\; T_y \;\; T_{xx} \;\; T_{xy} \;\; T_{yy}\}_P \tag{A2}$$

$$\mathbf{D}_T^{\mathrm{T}} = \{1 \;\; 0 \;\; \ldots \;\; 0\} \tag{A3}$$

$\mathbf{y}_T(2) = T_x$ and $\mathbf{y}_T(3) = T_y$ provide the temperature derivatives at the boundary to evaluate the boundary condition for the temperature sensitivity

$$s_T = \bar{T}' - \left(T_x \frac{\partial x_P}{\partial a} + T_y \frac{\partial y_P}{\partial a} \right) \quad (\Gamma_D^{\mathrm{T}}) \tag{A4}$$

Note that $\bar{T}'$, $\partial x_P/\partial a$ and $\partial y_P/\partial a$ are always problem dependent and provided by the user.

A.2. Neumann condition for the temperature

Consider now a Neumann boundary condition $\kappa \nabla T \cdot \hat{\mathbf{n}} = \overline{q_P}$ imposed at node P. The constrained least-squares problem (26) yields the linear system

$$\begin{bmatrix} \sum_{N\in\mathscr{P}} \mathbf{B}\mathbf{B}^{\mathrm{T}} & \mathbf{N}_T \\ \mathbf{N}_T^{\mathrm{T}} & 0 \end{bmatrix} \begin{Bmatrix} \mathbf{y}_T \\ l_T \end{Bmatrix} = \begin{Bmatrix} \sum_{N\in\mathscr{P}} \mathbf{B} T_N \\ \overline{q_P} \end{Bmatrix} \tag{A5}$$

with

$$\mathbf{N}_T^{\mathrm{T}} = \{0 \;\; \kappa \hat{n}_x \;\; \kappa \hat{n}_y \;\; 0 \;\; \ldots \;\; 0\} \tag{A6}$$

Entries 2–6 of $\mathbf{y}_T$ provide the first derivatives T_x and T_y, and second derivatives T_{xx}, T_{xy} and T_{yy} required to evaluate the Neumann boundary condition for the sensitivity of temperature

$$\begin{aligned}(\kappa'\nabla T + \kappa\nabla s_T)\cdot\hat{\mathbf{n}} = \bar{q}' &- \kappa\left(T_{xx}\frac{\partial x_P}{\partial a} + T_{xy}\frac{\partial y_P}{\partial a}\right)\hat{n}_x \\ &- \kappa\left(T_{yx}\frac{\partial x_P}{\partial a} + T_{yy}\frac{\partial y_P}{\partial a}\right)\hat{n}_y \\ &- \kappa\left(T_x\frac{\partial \hat{n}_x}{\partial a} + T_y\frac{\partial \hat{n}_y}{\partial a}\right), \quad (\Gamma_{\mathrm{N}}^{\mathrm{T}})\end{aligned} \tag{A7}$$

assuming that κ is a constant. If κ varies in space or depends on physical variables, the above expression becomes slightly more complex.

A.3. Dirichlet conditions for the flow

When Dirichlet boundary conditions for the flow $u = \overline{u_P}$ and $v = \overline{v_P}$ are imposed at node P, one constrained Taylor least-squares problem is solved for each velocity component. This procedure is identical to that just described for the temperature. Then, entries 2 and 3 of $\mathbf{y}_u$ and $\mathbf{y}_v$ provide the flow derivatives u_x, u_y, v_x and v_y at the boundary required to evaluate the boundary conditions for the flow sensitivities:

$$s_u = \bar{u}' - \left(u_x\frac{\partial x_P}{\partial a} + u_y\frac{\partial y_P}{\partial a}\right) \quad (\Gamma_{\mathrm{D}}^{u}) \tag{A8}$$

$$s_v = \bar{v}' - (v_x\frac{\partial x_P}{\partial a} + v_y\frac{\partial y_P}{\partial a}) \quad (\Gamma_{\mathrm{D}}^{v}) \tag{A9}$$

A.4. Neumann conditions for the flow

This case must be analysed with care. Indeed, Neumann boundary conditions for the flow at node P involve the pressure p and the first derivatives of both velocity components u and v

$$\begin{bmatrix} -p + 2\mu u_x & \mu(u_y + v_x) \\ \mu(u_y + v_x) & -p + 2\mu v_y \end{bmatrix} \begin{Bmatrix} \hat{n}_x \\ \hat{n}_y \end{Bmatrix} = \begin{Bmatrix} \overline{t_x}_P \\ \overline{t_y}_P \end{Bmatrix} \tag{A10}$$

Therefore, three least-squares problems must be solved in a coupled manner for the two velocity components and the pressure to ensure that the Taylor series for u, v, and p are consistent with the boundary conditions imposed on the flow. Our approach consists in minimizing the sum of the three quadratic forms $\mathscr{J}(\mathbf{y}_u)$, $\mathscr{J}(\mathbf{y}_v)$ and $\mathscr{J}(\mathbf{y}_p)$ subject to the two constraints

$$\{-\mathbf{y}_p(1) + 2\mu\mathbf{y}_u(2)\}\hat{n}_x + \mu\{\mathbf{y}_u(3) + \mathbf{y}_v(2)\}\hat{n}_y = \overline{t_x}_P \tag{A11}$$

$$\mu\{\mathbf{y}_u(3) + \mathbf{y}_v(2)\}\hat{n}_x + \{-\mathbf{y}_p(1) + 2\mu\mathbf{y}_v(3)\}\hat{n}_y = \overline{t_y}_P \tag{A12}$$

In this case, the functional to minimize reads

$$\begin{aligned}\text{Min}\ &\frac{1}{2}\sum_{N\in\mathscr{P}}(\mathbf{B}^{\mathrm{T}}\mathbf{y}_u-u_N)^2+\frac{1}{2}\sum_{N\in\mathscr{P}}(\mathbf{B}^{\mathrm{T}}\mathbf{y}_v-v_N)^2+\frac{1}{2}\sum_{N\in\mathscr{P}}(\mathbf{B}^{\mathrm{T}}\mathbf{y}_p-p_N)^2\\&+l_u(\mathbf{N}_{uu}^{\mathrm{T}}\mathbf{y}_u+\mathbf{N}_{uv}^{\mathrm{T}}\mathbf{y}_v+\mathbf{N}_p^{\mathrm{T}}\mathbf{y}_p-\overline{t_{xP}})+l_v(\mathbf{N}_{vu}^{\mathrm{T}}\mathbf{y}_u+\mathbf{N}_{vv}^{\mathrm{T}}\mathbf{y}_v+\mathbf{N}_p^{\mathrm{T}}\mathbf{y}_p-\overline{t_{yP}})\end{aligned}\tag{A13}$$

with

$$\begin{aligned}\mathbf{y}_u^{\mathrm{T}}&=\{u\ \ u_x\ \ u_y\ \ u_{xx}\ \ u_{xy}\ \ u_{yy}\}_P\\\mathbf{y}_v^{\mathrm{T}}&=\{v\ \ v_x\ \ v_y\ \ v_{xx}\ \ v_{xy}\ \ v_{yy}\}_P\\\mathbf{y}_p^{\mathrm{T}}&=\{p\ \ p_x\ \ p_y\ \ p_{xx}\ \ p_{xy}\ \ p_{yy}\}_P\\\mathbf{N}_{uu}^{\mathrm{T}}&=\{0\ \ 2\mu\hat{n}_x\ \ \mu\hat{n}_y\ \ 0\ \ \ldots\ \ 0\}\\\mathbf{N}_{uv}^{\mathrm{T}}&=\{0\ \ \mu\hat{n}_y\ \ 0\ \ \ldots\ \ 0\}\\\mathbf{N}_{up}^{\mathrm{T}}&=\{-\hat{n}_x\ \ 0\ \ \ldots\ \ 0\}\\\mathbf{N}_{vu}^{\mathrm{T}}&=\{0\ \ 0\ \ \mu\hat{n}_x\ \ 0\ \ \ldots\ \ 0\}\\\mathbf{N}_{uv}^{\mathrm{T}}&=\{0\ \ \mu\hat{n}_x\ \ 2\mu\hat{n}_y\ \ \ldots\ \ 0\}\\\mathbf{N}_{vp}^{\mathrm{T}}&=\{-\hat{n}_y\ \ 0\ \ \ldots\ \ 0\}\end{aligned}\tag{A14}$$

l_u and l_v are Lagrange multipliers. By setting the gradients of (A13) to zero, we obtain the coupled linear system to solve to determine $\mathbf{y}_u$, $\mathbf{y}_v$ and $\mathbf{y}_p$ that satisfy the flow boundary conditions at node P

$$\begin{bmatrix}\sum_{N\in\mathscr{P}}\mathbf{B}\mathbf{B}^{\mathrm{T}} & & & \mathbf{N}_{uu} & \mathbf{N}_{vu}\\ & \sum_{N\in\mathscr{P}}\mathbf{B}\mathbf{B}^{\mathrm{T}} & & \mathbf{N}_{uv} & \mathbf{N}_{vv}\\ & & \sum_{N\in\mathscr{P}}\mathbf{B}\mathbf{B}^{\mathrm{T}} & \mathbf{N}_{up} & \mathbf{N}_{vp}\\ \mathbf{N}_{uu}^{\mathrm{T}} & \mathbf{N}_{uv}^{\mathrm{T}} & \mathbf{N}_{up}^{\mathrm{T}} & & \\ \mathbf{N}_{vu}^{\mathrm{T}} & \mathbf{N}_{vv}^{\mathrm{T}} & \mathbf{N}_{vp}^{\mathrm{T}} & & \end{bmatrix}\begin{Bmatrix}\mathbf{y}_u\\ \mathbf{y}_v\\ \mathbf{y}_p\\ l_u\\ l_v\end{Bmatrix}=\begin{Bmatrix}\sum_{N\in\mathscr{P}}\mathbf{B}u_N\\ \sum_{N\in\mathscr{P}}\mathbf{B}v_N\\ \sum_{N\in\mathscr{P}}\mathbf{B}p_N\\ \overline{t_x}\\ \overline{t_y}\end{Bmatrix}\tag{A15}$$

Entries of $\mathbf{y}_u$, $\mathbf{y}_v$ and $\mathbf{y}_p$ provide the velocity and pressure boundary derivatives required to evaluate the CSE boundary conditions:

$$\begin{aligned}&\{-S_p+2\mu(S_u)_x+2\mu' u_x\}\hat{n}_x+\{\mu(S_u)_y+\mu(S_v)_x+\mu' u_y+\mu' v_x\}\hat{n}_y\\&\quad=\overline{t}'_{xP}-\{(-p_x+2\mu u_{xx})\hat{n}_x+\mu(u_{yx}+v_{xx})\hat{n}_y\}\frac{\partial x_P}{\partial a}\end{aligned}$$

$$-\{(-p_y+2\mu u_{xy})\hat{n}_x+\mu(u_{yy}+v_{xy})\hat{n}_y\}\frac{\partial y_P}{\partial a}$$
$$-\left\{(-p+2\mu u_x)\frac{\partial \hat{n}_x}{\partial a}+\mu(u_y+v_x)\frac{\partial \hat{n}_y}{\partial a}\right\} \tag{A16}$$

$$\{\mu(S_u)_y+\mu(S_v)_x+\mu' u_y+\mu' v_x\}\hat{n}_x+\{-S_p+2\mu(S_v)_y+2\mu' v_y\}\hat{n}_y$$
$$=\overline{t}'_{yP}-\{\mu(u_{yx}+v_{xx})\hat{n}_x+(-p_x+2\mu v_{yx})\hat{n}_y\}\frac{\partial x_P}{\partial a}$$
$$-\{\mu(u_{yy}+v_{xy})\hat{n}_x+(-p_y+2\mu v_{yy})\hat{n}_y\}\frac{\partial y_P}{\partial a}$$
$$-\left\{\mu(u_y+v_x)\frac{\partial \hat{n}_x}{\partial a}+(-p+2\mu v_y)\frac{\partial \hat{n}_y}{\partial a}\right\} \tag{A17}$$

assuming that μ is constant. Additional terms appear when $\mu=\mu(x,y)$ or if μ depends on physical variables as would be the case for non-Newtonian flows.

REFERENCES

1. Cacuci D. Sensitivity theory for nonlinear systems. I. Nonlinear functional analysis approach. *Journal of Mathematical Physics* 1981; **22**(12):2794.
2. Cacuci D. Sensitivity theory for nonlinear systems. II. Extensions to additional classes of responses. *Journal of Mathematical Physics* 1981; **22**(12):2803.
3. Li S, Petzold L. Adjoint sensitivity analysis for time-dependent partial differential equations with adaptive mesh refinement. *Journal of Computational Physics* 2004; **198**:310–325.
4. Turgeon É, Pelletier D, Borggaard J. A continuous sensitivity equation approach to optimal design in mixed convection. *Numerical Heat Transfer* 2000; **38**:869–885.
5. Turgeon É, Pelletier D, Borggaard J. Sensitivity and uncertainty analysis for variable property flows. *39th AIAA Aerospace Sciences Meeting and Exhibit*, Reno, NV, 2001; *AIAA Paper 2001-0139*.
6. Borggaard J, Verma A. On efficient solutions to the continuous sensitivity equation using automatic differentiation. *SIAM Journal on Scientific Computing* 2001; **22**:39–62.
7. Zienkiewicz OC, Zhu JZ. The superconvergent patch recovery and *a posteriori* error estimates. Part 1: the recovery technique. *International Journal for Numerical Methods in Engineering* 1992; **33**:1331–1364.
8. Pelletier D, Turgeon É, Etienne S, Borggaard J. Reliable sensitivity analysis via an adaptative sensitivity equation method. *3rd AIAA Theoretical Fluid Mechanics Meeting*, St Louis, MO, 2002; *AIAA Paper 2002-2758*.
9. Roache PJ. *Verification and Validation in Computational Science and Engineering*. Hermosa Publishers: Albuquerque, NM, 1998.
10. Pelletier D, Ilinca F. Adaptive remeshing for the k–ε model of turbulence. *AIAA Journal* 1997; **35**:640–646.
11. Pelletier D. Adaptive finite element computations of complex flows. *International Journal for Numerical Methods in Fluids* 1999; **31**:189–202.
12. Zienkiewicz OC, Zhu JZ. The superconvergent patch recovery and *a posteriori* error estimates. Part 2: error estimates and adaptivity. *International Journal for Numerical Methods in Engineering* 1992; **33**:1365–1382.
13. Peraire J, Vahdati M, Morgan K, Zienkiewicz O. Adaptive remeshing for compressible flow computations. *Journal of Computational Physics* 1987; **72**:449–466.
14. Belhamadia Y, Fortin A, Chamberland E. Anisotropic mesh adaptation for the solution of the Stefan problem. *Journal of Computational Physics* 2004; **194**:233–255.
15. Pelletier D, Roache P. CFD code verification and the method of manufactured solutions. *Proceedings of the 10th Annual Conference of the CFD Society of Canada*, Windsor, ON, 2001.

